nanomanufacturing

Communication

Nano-Titanium Oxide in Polymeric Contact Lenses: Short Communication

Lina Mohammed Shaker [1,*], Ahmed A. Alamiery [1,2,*], Mohd Takriff [3,1] and Wan Nor Roslam Wan Isahak [1]

1 Department of Chemical and Process Engineering, Faculty of Engineering and Built Environment, Universiti Kebangsaan Malaysia (UKM), Bangi 43600, Malaysia; wannorroslam@ukm.edu.my
2 Energy and Renewable Energies Technology Center, University of Technology, Baghdad 10001, Iraq
3 Chemical and Water Desalination Engineering Program, Collage of Engineering, University of Sharjah, Sharjah 26666, United Arab Emirates; sobritakriff@ukm.edu.my or mtakriff@sharjah.ac.ae
* Correspondence: p109960@siswa.ukm.edu.my (L.M.S.); dr.ahmed1975@ukm.edu.my (A.A.A.); Tel.: +60-10-282-5186 (L.M.S.); +964-771-399-5509 (A.A.A.)

Abstract: Many individuals suffer from myopia or hyperopia and astigmatism owing to the refractive defects of the eye optics or because of the use of inappropriate contact lenses. This study dealt with three polymers Poly(methyl methacrylate) (PMMA), Poly(Hydroxyl methacrylate) (PHEMA), and Poly(glycidyl methacrylate) (PGMA) and doping them with TiO_2 nanoparticles to evaluate the difference between the effect of each lens on the human eye. The TiO_2 NPs were prepared in this work by the sol–gel method to obtain 70–90 nm sized particles. Modulation transfer (MTF) and spot diagram were assessed to measure ocular performance. The PGMA-TiO_2 contact lens provided the highest image quality at the lowest probability (P) of about $p < 0.0001$ when inserted on an aberrated eye system because of its ability to eliminate the chromatic aberrations created inside the eyes having a smaller spot size.

Keywords: contact lens; PMMA-TiO_2; PHEMA-TiO_2; PGMA-TiO_2; high refractive index

Citation: Shaker, L.M.; Alamiery, A.A.; Takriff, M.; Wan Isahak, W.N.R. Nano-Titanium Oxide in Polymeric Contact Lenses: Short Communication. *Nanomanufacturing* **2022**, 2, 71–81. https://doi.org/10.3390/nanomanufacturing2030006

Academic Editor: Andres Castellanos-Gomez

Received: 8 June 2022
Accepted: 28 June 2022
Published: 30 June 2022

1. Introduction

Medical contact lenses are used to correct refractive errors and treat visual deficiencies. The soft toric, rigid gas permeable (RGP), and mini-scleral lenses have been particularly effective in improving vision in patients with high or irregular astigmatism, keratoconus (KCN), and damaged or scarred corneas. Today, more than 88% of the world's contact lens wearers use soft contact lenses, while the remaining approximately 12% use gas permeable (hard or rigid) contact lenses [1]. Soft contact lenses are typically prescribed under specific state laws in the United States by specifying the brand, base curve, diameter, and power. The use of contact lenses, however, has often been associated with some unwanted alterations in the cornea [2]. Those alterations have been driven by several factors including mechanical stress and altered corneal metabolism as a result of hypoxia and hypercapnia [3]. The adverse effects of wearing contact lenses can appear in all layers of the cornea, that is, the epithelium (e.g., microcysts and changes in junctional integrity), the stroma (e.g., stromal edema and stromal acidosis), and the endothelium (e.g., bleb formation and polymegethism) [4]. When prescribing contact lenses, there are many factors to be considered, including occupational and lifestyle needs of the wearer, use of digital devices, and type of work environment. For patients who participate in sporting activities, knowledge of the environmental conditions is required, that is, exposure to dust, water, temperature, altitude, and UV, as well as body movement and contact involved in that sport [5]. One must also consider convenience, ease of use, handling capability, and budget of the wearer, and therefore, a thorough case history is essential [6].

For more than 60 years, companies producing contact lenses have been manufacturing lenses from a mixture of polymers with different properties to obtain a comfortable lens that is suitable for human eye tissue [7]. Comfort can change dramatically from one lens brand to another due to a number of factors, including the material, peripheral lens design, thickness, and the shape of the edge [8]. This is important, as lens comfort is the major reason for patients' discontinuation of contact lens wear [9].

When evaluating a contact lens physically, the refractive index (n) is often used as a criterion for evaluation in addition to the Abbe number (ν_d), the flexibility of the lens, and whether it is hydrophilic or hydrophobic [10]. As it is known, the lens is a refractive surface that has a certain n value according to the materials it is made of. Previous researchers have resorted to increasing n in various ways, including doping the polymer with metal oxides such as TiO_2 [3], ZnO [4], Al_2O_3 [5], and other nanoparticles (NPs) [6]. However, manufacturers still rely on a refractive index that is lower than the refractive index of the corneal surface, which means that these lenses have a high dispersion index, which increases the possibility of aberrations being generated in the image formed on the retina. The use of TiO_2 in medicine extends beyond the development of drug delivery methods and the use of chemotherapeutic vehicles [11–15]. Particle type, surface charge, surface coating, size, dose, and exposure route all affect the pharmacokinetics of metal NPs, including TiO_2 [16]. TiO_2 NPs have been used due to their bioavailability in pharmacy [17], particularly in pharmaceutical chemistry and technology [18], as well as in medicine [19], particularly in the rapidly increasing fields of dentistry and surgery. The TiO_2 forms are chosen for possible dental, surgical, and pharmaceutical uses. This study dealt with three polymers Poly(methyl methacrylate) (PMMA), Poly(Hydroxyethyl methacrylate) (PHEMA), and Poly(glycidyl methacrylate) (PGMA) and doping them with TiO_2 NPs to evaluate the difference between the effect of each lens on human vision.

2. Materials and Methods

PMMA of 99% purity was obtained from interchimiques SA, France. HEMA and PGMA of purity > 99% were obtained from Sigma Aldrish, Selangor, Malaysia. TiO_2 NPs were prepared using the sol–gel method [20]. Tetra butyl titanate (Ti-(OC_4H_9)) was dissolved with absolute ethanol and contained in acetone and acetic acid. The mixture was left dark with constant shaking for 30 min. After that, a mixture of pure ethanol with non-ionic water was added with continuous shaking for 2 h. Note that the initial ratio of Ti(OC_4H_9) reactants by 1 mol, 30 mL ethanol, 3 mL water, 2 mol acetic acid, and 1 mol acetone was followed by filtration, drying, and burning at 550 °C. Chloroform was used to dissolve the PMMA, PHEMA, and PGMA polymers. A total of 10 mL of an ethanol and xylene mixture (50:50) was dissolved with 0.1 g TiO_2 NPs to obtain the doped PMMA-TiO_2, PHEMA-TiO_2, and PGMA-TiO_2 contact lenses at 0.005 w/v. Scanning electron microscopy (SEM) was performed by SEM 54032-GE02-0002/8038 (MIRA3/Austria) for morphological characterization. The refractive index was measured by an Abbe refractometer at wavelengths 486.1, 587.6, and 656.3 nm, whereas the Abbe number was calculated using the following formula [21]:

$$v_d = \frac{(n_D - 1)}{(n_F - n_C)} \tag{1}$$

ν_d: Abbe number, and n_C, n_D, and n_F are the refractive indices of the polymer films at wavelengths of 656, 589, and 486 nm, respectively. After measuring and calculating n and υ_d of each lens, the lenses were inserted on the aspherical corneal surface of the Liou and Brennan eye model [22] and modeled by ZEMAX 13-Realease 2 SPA4 software with input parameters shown in Figure 1 [23].

Optical properties of these nanocomposites were measured by UV–Vis transmission spectroscopy UV-1601 PC (Shimadzu/Japan). All of the prepared nanomaterial structures were investigated by the X-ray diffraction (XRD) pattern by Philips XPERT-MPD diffractometer and Scherrer equation to calculate the crystallite size (D) [24]:

$$D = \frac{k\lambda}{\beta \cos\theta} \tag{2}$$

where $k = 0.9$ is a dimensionless geometric factor that accounts for the particle shape, $\lambda_{\mathrm{CuK}\alpha}$ is 1.54 nm, β is the full width at half maximum (FWHM) of the most intense diffraction peak, and θ is the diffraction angle. TiO_2 NPs were weighed by analytical balance from AS Radwag 220/C/2, and the magnetic stirrer was used to agitate the solution for speeding up the reactions and improving mixtures.

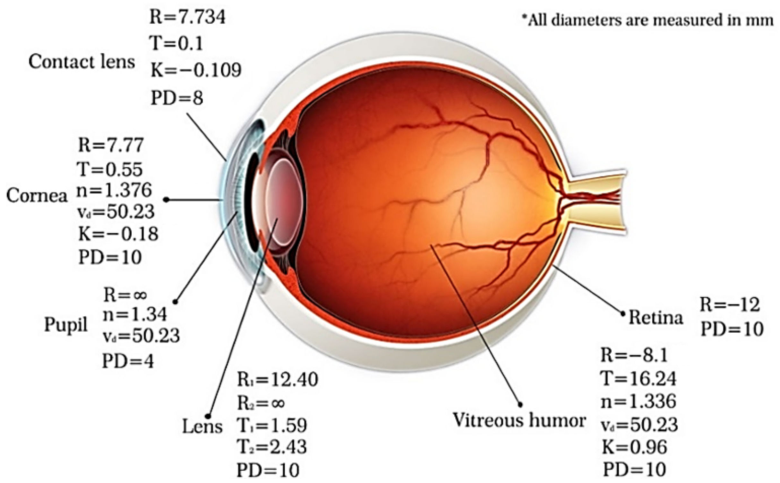

Figure 1. ZEMAX software parameters in. R: the radius of curvature of each surface, T: thickness of each surface, K: the conic constant, PD: entrance pupil diameter, and R1, R2, T1, and T2 are the front radius of curvature, back radius of curvature, front surface thickness, and back surface thickness of the crystalline lens, respectively.

3. Results

First of all, in this paper, PMMA, PHEMA, and PGMA were tested and doped with a range of TiO_2 NP concentrations from 0.0001, 0.005, 0.0075, to 0.01 w/v. Through laboratory testing, it was found that the best properties were obtained in all nanocomposites when using a concentration of 0.005 w/v. When the NP percentage was high, the films were less transparent and had a dotted surface, while the lowest percentage was unsuccessful in terms of raising the refractive index of the nanocomposites used. The prepared samples of the mentioned concentrations for PMMA-TiO_2, PHEMA-TiO_2, and PGMA-TiO_2 are shown in Figure 2. TiO_2 NPs are considered biologically inert according to international classifications with human and animal tissues. Additionally, TiO_2 NPs are a natural material that has relative acceptance by the public [25]. XRD analysis is a commonly used technique to assess the crystallinity of metals and non-metals [26]. The TiO_2 NP size was calculated from Equation (2) for more confirmation. All the patterns of the prepared samples were plotted in one graph to illustrate and compare the shift in peaks due to the doping. The XRD patterns of the prepared bulk TiO_2 and the PMMA-TiO_2, PHEMA-TiO_2, and PGMA-TiO_2 nanocomposite specimens were recorded at 40 KV and 40 mA and plotted within the range $10° \leq 2\theta \leq 90°$ in Figure 3. As shown, the wide bands indicate the presence of crystalline TiO_2 NPs.

To find out the spectral transmittance of each of the prepared samples, the transmittance data for the range of 300–800 nm were recorded by UV–Vis transmission spectroscopy using UV-1601 PC. In research dealing with the subject of medical contact lenses, it is necessary to know whether this lens works to block UV rays from the eye through this analysis [27]. Figure 4 shows the effect of doping PMMA, PHEMA, and PGMA with TiO_2 NPs on visible light transmittance and UV blocking. PMMA-TiO_2 recorded $\geq$96% of light transmittance in this work. Random areas in each sample were selected to study the surface morphology by means of SEM. However, the homogeneity of the nanomaterial was clear through its effect on the ability of the prepared films to block UV light and pass visible light. UV spectroscopy can give the researchers a rough idea of the homogeneity or heterogeneity of a nanocomposite as the homogeneous nanocomposites follow the Beer–Lambert law, while the heterogeneous nanocomposites show deviations from the Beer–Lambert law because of the phenomena of absorption and transmittance. SEM images illustrated the morphological topography of each sample. Figure 5 illustrates the surface morphology characteristics of the prepared samples through the SEM images at different magnifications. In this figure, different sizes and shapes of TiO_2 NPs appeared imbedded in the polymer matrices.

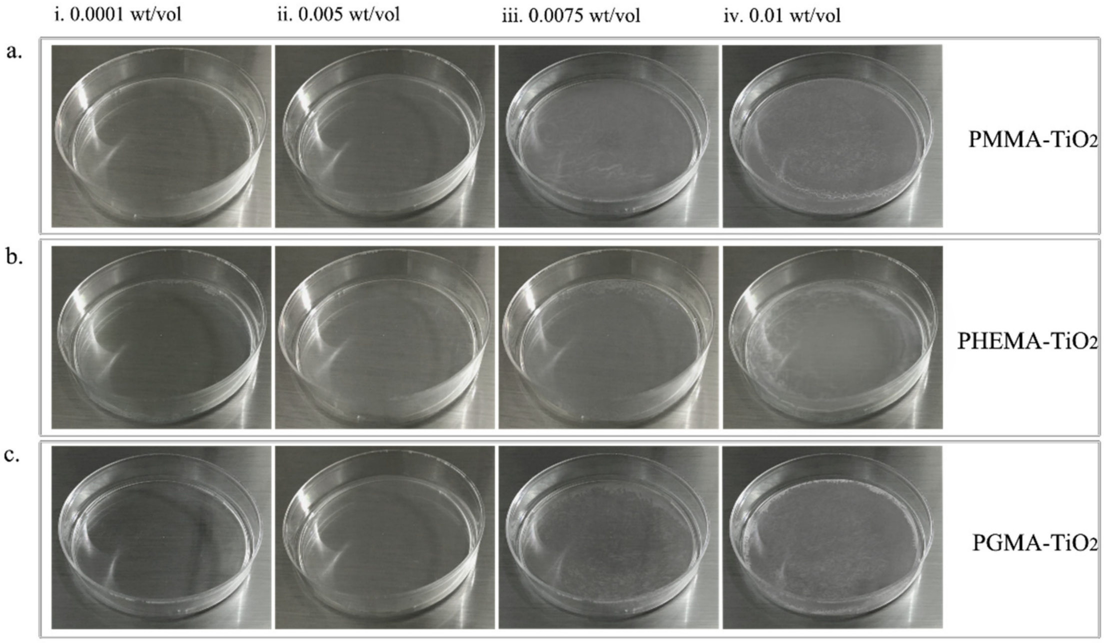

Figure 2. The prepared samples in the laboratory to choose the best TiO_2 NP concentration of (**a**) PMMA-TiO_2, (**b**) PHEMA-TiO_2, and (**c**) PGMA-TiO_2. Each nanocomposite was prepared in the four concentrations: i. 0.0001 w/v, ii. 0.005 w/v, iii. 0.0075 w/v, and iv. 0.01 w/v.

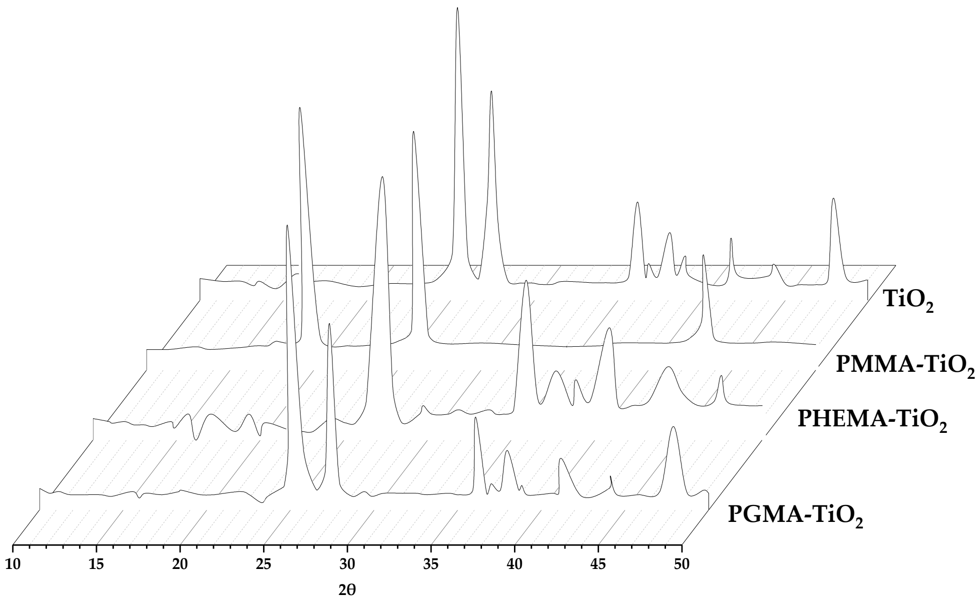

Figure 3. XRD patterns of blank TiO_2, PMMA-TiO_2, PHEMA-TiO_2, and PGMA-TiO_2.

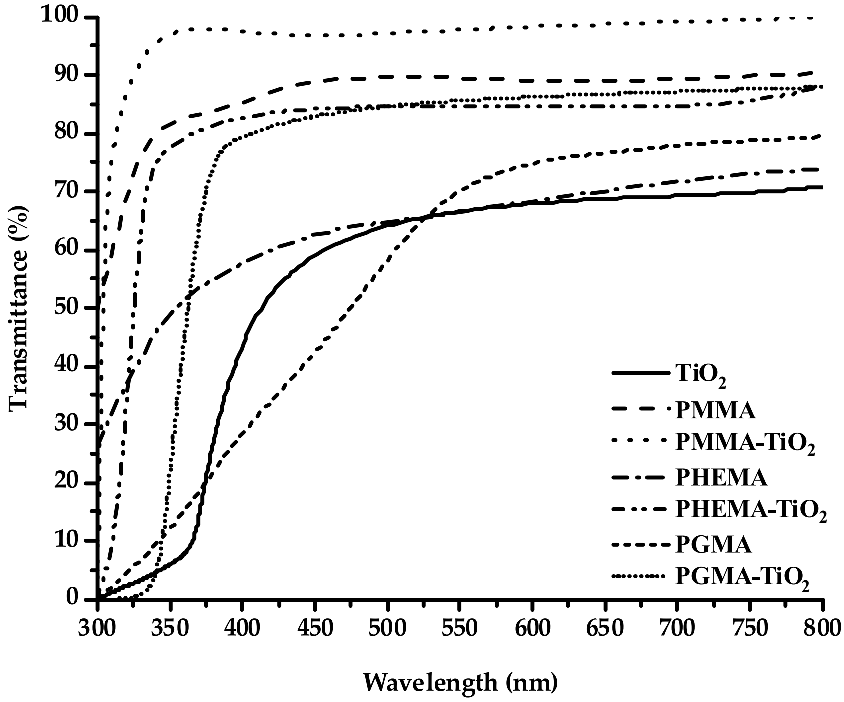

Figure 4. UV–Vis transmittance of blank TiO_2, pure PMMA, PHEMA, and PGMA polymers, and doped nanocomposites PMMA-TiO_2, PHEMA-TiO_2, and PGMA-TiO_2.

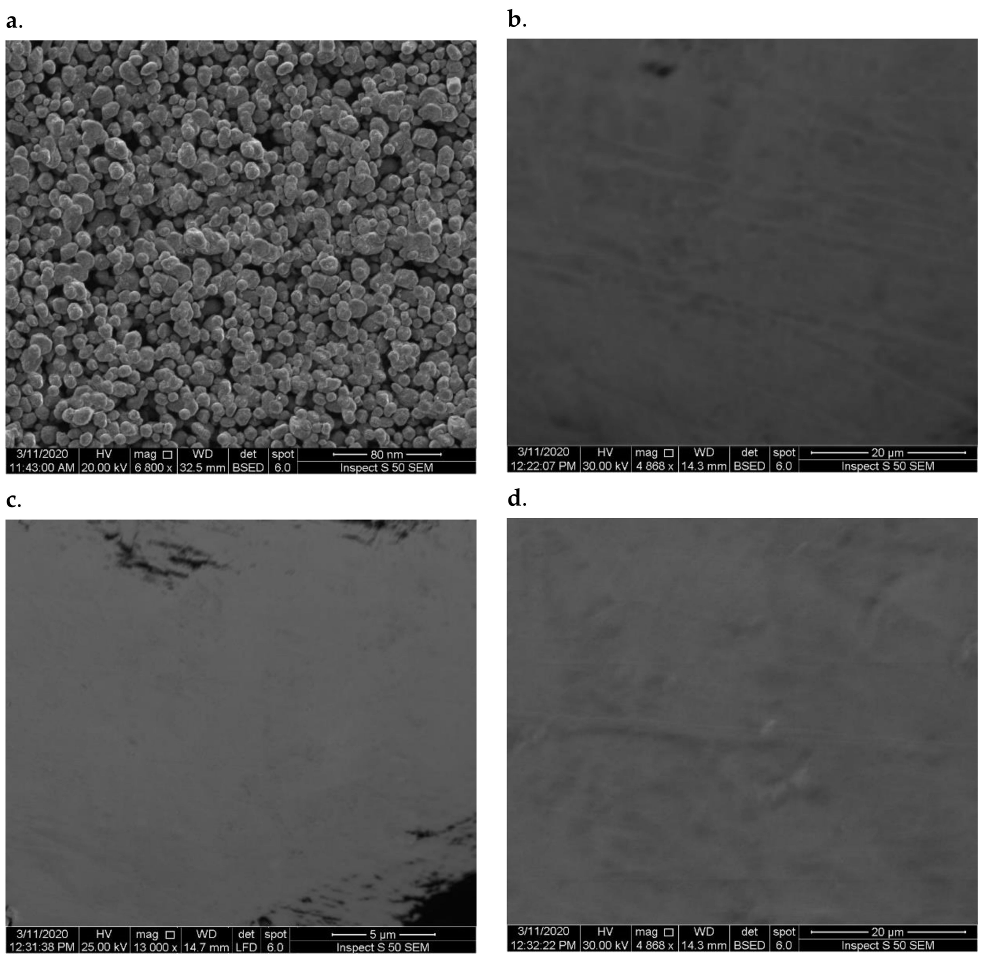

Figure 5. *Cont.*

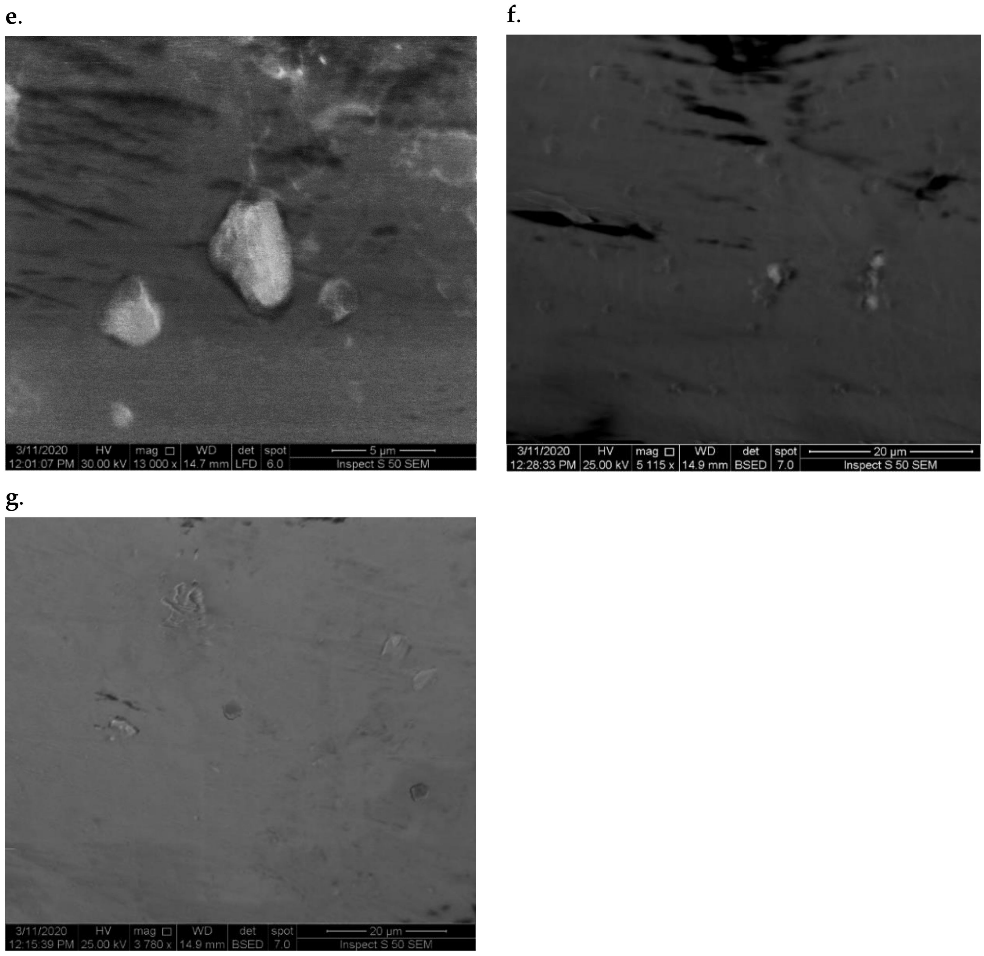

Figure 5. SEM images for (**a**) TiO_2 NPs, (**b**) PMMA, (**c**) PHEMA, (**d**) PGMA, (**e**) PMMA-TiO_2, (**f**) PHEMA-TiO_2, and (**g**) PGMA-TiO_2.

The refractive index curves of each of the three polymers were plotted before and after doping with TiO_2 NPs as a function of wavelength (in nm) with a range 480–660 nm [28]. The graphs were inserted under the MTF chart to show the relationship of the refractive index for improving or worsening the MTF function, which refers to the dissipation of energy spread on the retina as illustrated from the spot diagram [29]. Figure 6a shows the worst retinal images that were achieved when the pure polymers were applied as CLs because of their low index of refraction. Figure 6b clearly proves that all of the hybrid contact lenses had good contrast at low frequencies (less than 20 cycles/mm) and degradation of the contrast over 0.5; this is clear from the smaller spot size accumulated on the retina shown in Figure 6c.

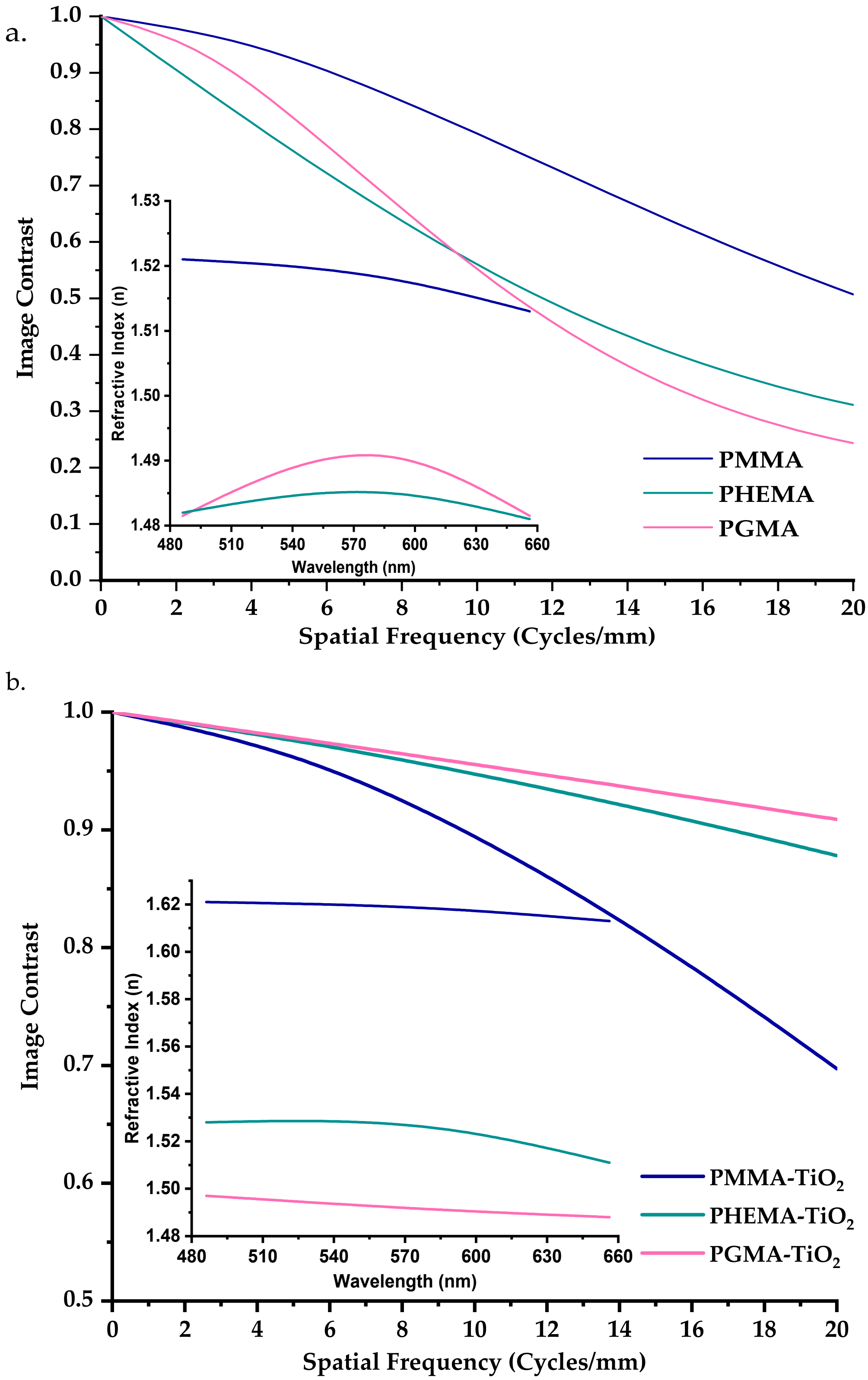

Figure 6. *Cont.*

c.

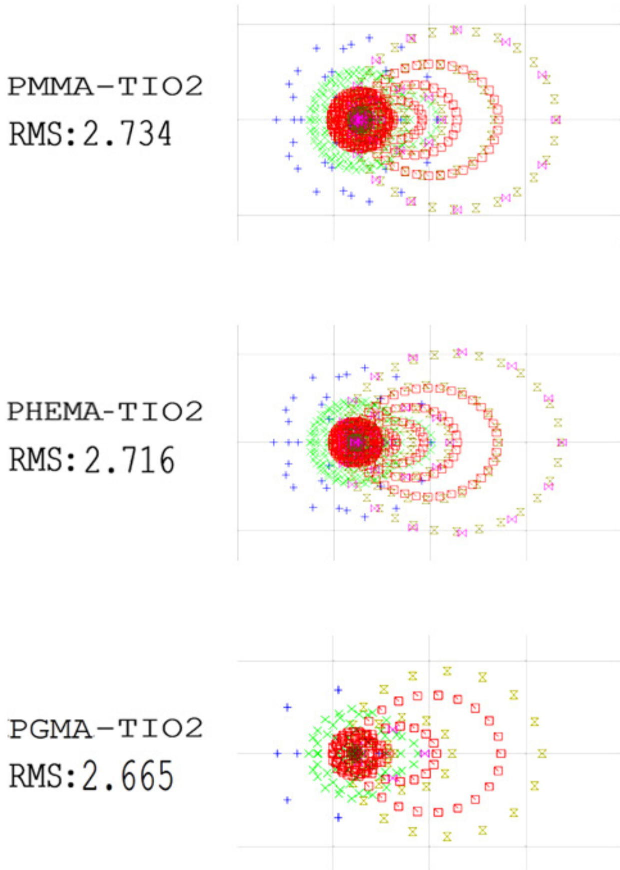

Figure 6. Polychromatic MTF simulation curves of (**a**) prepared contact lenses, (**b**) TiO_2 NP-doped contact lenses, and (**c**) the spot diagram of the prepared contact lenses.

4. Discussion

XRD patterns were recorded on a Philips XPERT-MPD diffractometer to evaluate the modification of the polymer matrix after doping them with the TiO_2 NPs to increase their refractive indices [26]. TiO_2 NPs of 70–90 nm were characterized with the anatase phase peaks appearing in Figure 3 at 25.5°, 37.7°, and 48.2° which belong to the planes (101), (004), and (200), respectively. PMMA-TiO_2 that found 2θ = 26.04°, 42.95°, and 57.03 were assigned to (100), (101), and (111) planes, respectively. However, both PHEMA-TiO_2 and PGMA-TiO_2 had no significance shift in their patterns [30].

All of the nanocomposites were highly transparent in the visible range after doping them with TiO_2 NPs. Transmittance of all films was higher than 95%, indicating the homogeneity and compatibility of doping PMMA with TiO_2 NPs [31]. Figure 4 shows that due to the effect of doping PMMA with TiO_2 NPs, the transmittance percentage reduced to 98–96% [32]. However, the prepared nanocomposites were transparent and maintained value of transmittance above 95% in the visible region. The observed higher transmittance for the prepared PMMA-TiO_2 nanocomposites was much better than what had been obtained in some previous investigations [33]. Theses lenses worked as a UV blocker due to lower transmittance values in the UV region. This agrees with the results of a previous investigation [34]. Both PHEMA-TiO_2 and PGMA-TiO_2 contact lenses showed the same light transmission indication in blocking the UV region which was less than the PMMA-TiO_2 lens due to the scattering generated from agglomerating the TiO_2 NPs during the preparation. The change in n values at 486.10 nm, 587.60 nm, and 656.30 nm was attributed to the dispersal phenomenon. This alternation-produced hybrid nanocomposite ν_d values for the samples were obtained at 31.00, 54.00, and 60.80 for PMMA-TiO_2, PHEMA-TiO_2, and PGMA-TiO_2 contact lenses, respectively. The effect of the epoxy group on the optical properties of the PGMA-TiO_2 composite could be summarized as highly transparent in the whole visible range [35], exhibiting a transparency of approximately 90%. The sharp UV–Vis transmittance spectra onsets also indicated that TiO_2 nanocomposites do not scatter light to any appreciable extent in the visible range. When preparing high refractive index nanocomposites, the concern for transparency loss is primarily due to scattering by nanoparticles within organic polymers.

The surface morphology of 0.005 w/v PMMA-TiO_2, PHEMA-TiO_2, and PGMA-TiO_2 specimens at different magnifications are shown in Figure 5. Different sizes and shapes of TiO_2 NPs were embedded in the PMMA, PHEMA, and PGMA polymer samples; the pure PMMA, PHEMA, and PGMA. The polymers' morphological images are shown in Figure 5b–d. According to the prepared TiO_2 NP characterization, the XRD patterns showed a TiO_2 NP crystallite size of 70–90 nm with a particle size range of 10–30 nm (see Figure 5a). XRD measures the grain size using the Scherrer equation but SEM measures particle size. Some areas on the surface of the PMMA-TiO_2 sample in Figure 5e clearly show the doping of the polymer and the homogeneity of the nanomaterial within the polymer matrix [32]. Due to the agglomeration of TiO_2 NPs in the PHEMA network as shown in the SEM image in Figure 5f, the transmittance of visible light in this sample decreased due to making these particles an obstacle to the passage of light in one direction. Finally, Figure 5g shows a more homogeneous distribution of TiO_2 NPs and more surface adhesion with PGMA than with PHEMA [36]. Most medical contact lenses depend in their installation on the use of PHEMA as a basic polymer in their manufacture [37], but the physical problems resulting from it make contact lenses made of them less desirable because of related complications, visual problems, and discomfort it causes when wearing [2].

MTF criteria were used to characterize retinal image sharpness and contrast [38]. In Figure 6a,b, the difference in the area under the curve shows that the best effect of metal nanoparticles appeared when mixed with PGMA with 2.665 spot size, which gave the highest image clarity and which approached the response of the diffraction limit, representing the ideal vision system. From the spot diagram and n value at each wavelength presented in Figure 6c, we concluded that the chromatic aberration generated as a result of high ν_d values was responsible for the decay of the MTF curve for PMMA-TiO_2 and PHEMA-TiO_2, and consequently, for the increase in the size of the spot in which the image was focused on the retina [39]. The refractive index indication of the prepared nanocomposites increased with increasing TiO_2 NP concentration due to the polymer density increment (n = c/v), whereas ν_d values exhibited an opposite trend. Such refractive indices are superior to commercial CLs (1.43) as well as those reported by others [34] using different polymers [40]. This discussion above encourage researchers to raise the index of refraction and maintain the balance with the dispersion coefficient by choosing a TiO_2 concentration of 0.005 w/v.

5. Conclusions

Light transmission across the light spectrum may vary from material to material for several reasons, including whether they have UV blocking capabilities. The prepared transparent TiO_2-doped nanocomposites showed acceptable features to be used in manufacturing a medical contact lens. Contact lens manufacturers still rely on a refractive index that is lower than the refractive index of the corneal surface, which means that these lenses have a high dispersion index that increases the possibility of generating an aberrated image. This study dealt with doping PMMA, PHEMA, and PGMA with TiO_2 NPs for evaluating the difference between the effect of each lens on human eye vision supported by a theoretical study based on the design of the Liou and Brennan eye model using ZEMAX 13-Realease 2 SPA4 optical design. From this study, we concluded that TiO_2

is a good candidate for raising the n value of the lens to close to the refractive index of human eye tissue. This in turn enables the lens to eliminate distortions that occur as a result of scattering and optical refractions. The higher image quality showed a smaller spot size in the spot diagram because some of the rays accumulated in distant points from the spot center on the retina. Taking into account the selection of a proper polymer is necessary to maintain a balance between n and ν_d.

Author Contributions: Conceptualization, A.A.A. and L.M.S.; methodology, A.A.A. and L.M.S.; software, L.M.S.; validation, W.N.R.W.I. and M.T.; formal analysis, L.M.S.; investigation, A.A.A. and L.M.S.; resources, W.N.R.W.I. and M.T.; data curation, L.M.S.; writing—original draft preparation, A.A.A. and L.M.S.; writing—review and editing, A.A.A.; visualization, M.T.; supervision, A.A.A., W.N.R.W.I. and M.T.; project administration, A.A.A., W.N.R.W.I. and M.T.; funding acquisition, W.N.R.W.I. and M.T. All authors have read and agreed to the published version of the manuscript.

Funding: This research was funded by Universiti Kebangsaan Malaysia under grant FRGS/1/2020/TK0/UKM/02/31, Funded by Ministry of Higher Education Malaysia.

Informed Consent Statement: Not applicable.

Data Availability Statement: The data of this study are available from the corresponding author (A.A.) upon reasonable request.

Acknowledgments: The authors thank Universiti Kebangsaan Malaysia (Malaysia) and University of Technology (Iraq) for supporting this work.

Conflicts of Interest: The authors declare no conflict of interest.

References

1. Morgan, P.B.; Efron, N.; Woods, C.A.; Santodomingo-Rubido, J. International survey of orthokeratology contact lens fitting. *Contact Lens Anterior Eye* **2018**, *42*, 450–454. [CrossRef]
2. Alipour, F.; Khaheshi, S.; Soleimanzadeh, M.; Heidarzadeh, S.; Heydarzadeh, S. Contact Lens-related Complications: A Review. *J. Ophthalmic Vis. Res.* **2017**, *12*, 193–204. [CrossRef]
3. Ohta, K.; Shimamura, I.; Shiraishi, A.; Ohashi, Y. Confocal Microscopic Observations of Stromal Keratocytes in Soft and Rigid Contact Lens Wearers. *Cornea* **2012**, *31*, 66–73. [CrossRef]
4. Liesegang, T.J. Physiologic changes of the cornea with contact lens wear. *CLAO J.* **2002**, *28*, 12–27.
5. Bennett, E.S.; Weissman, B.A. *Clinical Contact Lens Practice*; Lippincott Williams & Wilkins: Philadeplhia, PA, USA, 2005; pp. 475–477.
6. Bennett, E.S.; Vinita, A.H. *Clinical Manual of Contact Lenses*, 4th ed.; Lippincott Williams & Wilkins: Philadeplhia, PA, USA, 2015.
7. Brennan, N.A.; Efron, N.; Bruce, A.S.; Duldig, D.I.; Russo, N.J. Dehydration of hydrogel lenses: Environmental influences during normal wear. *Am. J. Optom. Physiol. Opt.* **1988**, *65*, 277–281. [CrossRef]
8. Turhan, S.; Toker, E. Optical coherence tomography to evaluate the interaction of different edge designs of four different silicone hydrogel lenses with the ocular surface. *Clin. Ophthalmol.* **2015**, *9*, 935–942. [CrossRef] [PubMed]
9. Richdale, K.; Sinnott, L.T.; Skadahl, E.; Nichols, J.J. Frequency of and Factors Associated with Contact Lens Dissatisfaction and Discontinuation. *Cornea* **2007**, *26*, 168–174. [CrossRef] [PubMed]
10. Musgrave, C.S.A.; Fang, F. Contact Lens Materials: A Materials Science Perspective. *Materials* **2019**, *12*, 261. [CrossRef] [PubMed]
11. Shaker, L.M.; Al-Amiery, A.A.; Kadhum, A.A.H.; Takriff, M.S. Manufacture of Contact Lens of Nanoparticle-Doped Polymer Complemented with ZEMAX. *Nanomaterials* **2020**, *10*, 2028. [CrossRef]
12. Demir, M.M.; Koynov, K.; Akbey, Ü.; Bubeck, C.; Park, I.; Lieberwirth, A.I.; Wegner, G. Optical Properties of Composites of PMMA and Surface-Modified Zincite Nanoparticles. *Macromolecules* **2007**, *40*, 1089–1100. [CrossRef]
13. Al-Obaidi, A.A.; Salman, A.J.; Yousif, A.R.; Al-Mamoori, D.H.; Mussa, M.H.; Gaaz, T.S.; Kadhum, A.A.H.; Takriff, M.S.; Al-Amiery, A.A. Characterization the effects of nanofluids and heating on flow in a baffled vertical channel. *Int. J. Mech. Mater. Eng.* **2019**, *14*, 11. [CrossRef]
14. Xu, J.; Zhang, Y.; Zhu, W.; Cui, Y. Synthesis of Polymeric Nanocomposite Hydrogels Containing the Pendant ZnS Nanoparticles: Approach to Higher Refractive Index Optical Polymeric Nanocomposites. *Macromolecules* **2018**, *51*, 2672–2681. [CrossRef]
15. Wang, T.; Jiang, H.; Wan, L.; Zhao, Q.; Jiang, T.; Wang, B.; Wang, S. Potential application of functional porous TiO2 nanoparticles in light-controlled drug release and targeted drug delivery. *Acta Biomater.* **2015**, *13*, 354–363. [CrossRef]
16. Carlander, U.; Li, D.; Jolliet, O.; Emond, C.; Johanson, G. Toward a general physiologically-based pharmacokinetic model for intravenously injected nanoparticles. *Int. J. Nanomed.* **2016**, *11*, 625–640. [CrossRef]
17. Carp, O.; Huisman, C.L.; Reller, A. Photoinduced reactivity of titanium dioxide. *Prog. Solid State Chem.* **2004**, *32*, 33–177. [CrossRef]

18. Hautala, J.; Kääriäinen, T.; Hoppu, P.; Kemell, M.; Heinämäki, J.; Cameron, D.; George, S.; Juppo, A.M. Atomic layer deposition—A novel method for the ultrathin coating of minitablets. *Int. J. Pharm.* **2017**, *531*, 47–58. [CrossRef]
19. Razavi, H.; Janfaza, S. Medical nanobiosensors: A tutorial review. *Nanomed. J.* **2015**, *2*, 74–87. Available online: http://nmj.mums.ac.ir (accessed on 24 June 2022).
20. Kamil, F.; Hubiter, K.A.; Abed, T.K.; Al-Amiery, A.A. Synthesis of Aluminum and Titanium Oxides Nanoparticles via Sol-Gel Method: Optimization for the Minimum Size. *J. Nanosci. Technol.* **2016**, *2*, 37–39.
21. Schaub, M.; Schwiegerling, J.; Fest, E.C.; Symmons, A.; Shepard, R.H. *Molded Optics: Design and Manufacture*; Taylor and Francis Group LLC: Oxfordshire, UK, 2011.
22. Liou, H.-L.; Brennan, N.A. Anatomically accurate, finite model eye for optical modeling. *J. Opt. Soc. Am. A* **1997**, *14*, 1684–1695. [CrossRef]
23. Dua, S.; Acharya, R.; Ng, E.Y.K. *Computational Analysis of the Human Eye with Applications*; World Scientific: Singapore, 2011. [CrossRef]
24. Scherrer, P. Bestimmung der inneren Struktur und der Größe von Kolloidteilchen mittels Röntgenstrahlen. In *Kolloidchemie Ein Lehrbuch*; Springer: Berlin/Heidelberg, Germany, 1912; pp. 387–409.
25. Jin, T.; Costa, M.; Chen, X. Titanium. In *Handbook on the Toxicology of Metals*, 5th ed.; Elsevier Inc: Amsterdam, The Netherlands, 2021; pp. 857–868.
26. Bunaciu, A.A.; Udriştioiu, E.G.; Aboul-Enein, H.Y. X-ray Diffraction: Instrumentation and Applications. *Crit. Rev. Anal. Chem.* **2014**, *45*, 289–299. [CrossRef]
27. Filipecki, J.; Kocela, A.; Korzekwa, P.; Miedzinski, R.; Filipecka-Szymczyk, K.; Golis, E. Structural study of polymer hydrogel contact lenses by means of positron annihilation lifetime spectroscopy and UV–Vis–NIR methods. *J. Mater. Sci. Mater. Med.* **2013**, *24*, 1837–1842. [CrossRef]
28. Nakayama, N.; Hayashi, T. Preparation and characterization of TiO_2 and polymer nanocomposite films with high refractive index. *J. Appl. Polym. Sci.* **2007**, *105*, 3662–3672. [CrossRef]
29. Watson, A.B. A formula for the mean human optical modulation transfer function as a function of pupil size Computing the mean radial MTF. *J. Vis.* **2013**, *13*, 18. [CrossRef]
30. Tao, P.; Li, Y.; Rungta, A.; Viswanath, A.; Gao, J.; Benicewicz, B.C.; Siegel, R.W.; Schadler, L.S. TiO_2 nanocomposites with high refractive index and transparency. *J. Mater. Chem.* **2011**, *21*, 18623–18629. [CrossRef]
31. Gnanaseelan, M.; Kalita, U.; Janke, A.; Pionteck, J.; Voit, B.; Singha, N.K. All methacrylate block copolymer/TiO_2 nanocomposite via ATRP and in-situ sol-gel process. *Mater. Today Commun.* **2019**, *22*, 100728. [CrossRef]
32. Xi, Y.; Qi, Y.; Mao, Z.; Yang, Z.; Zhang, J. Surface hydrophobic modification of TiO_2 and its application to preparing PMMA/TiO_2 composite cool material with improved hydrophobicity and anti-icing property. *Constr. Build. Mater.* **2020**, *266*, 120916. [CrossRef]
33. Maldonado-Codina, C.; Efron, N. Dynamic wettability of pHEMA-based hydrogel contact lenses. *Ophthalmic Physiol. Opt.* **2006**, *26*, 408–418. [CrossRef]
34. Sugumaran, S.; Bellan, C. Transparent nano composite PVA–TiO_2 and PMMA–TiO_2 thin films: Optical and dielectric properties. *Optik* **2014**, *125*, 5128–5133. [CrossRef]
35. Tao, P.; Viswanath, A.; Li, Y.; Siegel, R.W.; Benicewicz, B.C.; Schadler, L.S. Bulk transparent epoxy nanocomposites filled with poly(glycidyl methacrylate) brush-grafted TiO_2 nanoparticles. *Polymer* **2013**, *54*, 1639–1646. [CrossRef]
36. Opdahl, A.; Kim, S.H.; Koffas, T.S.; Marmo, C.; Somorjai, G.A. Surface mechanical properties of pHEMA contact lenses: Viscoelastic and adhesive property changes on exposure to controlled humidity. *J. Biomed. Mater. Res.* **2003**, *67*, 350–356. [CrossRef]
37. Saptaji, K.; Iza, N.R.; Widianingrum, S.; Mulia, V.K.; Setiawan, I. Poly(2-Hydroxyethyl Methacrylate) Hydrogels for Contact Lens Applications—A Review. *Makara J. Sci.* **2021**, *25*, 3. [CrossRef]
38. Hecht, E. *Optics*, 5th ed.; Pearson Education Limited: London, UK, 2017.
39. Castejon-Mochon, J.F.; Lopez-Gil, N.; Benito, A.; Artal, P. Ocular wave-front aberration statistics in a normal young population. *Vis. Res.* **2002**, *42*, 1611–1617. [CrossRef]
40. Seinder, L.; Spinelli, H.J.; Ali, M.I.; Weintraub, L. Silicone-Containing Contact Lens Polymers, Oxygen Permeable Contact Lenses and Methods for Making There Lenses and Treating Patients with Visual Impairment. U.S. Patent 5331067, 19 July 1994.